NANO LETTERS

2007
Vol. 7, No. 2
338−344

Deciphering the Kinetic Mechanism of Spontaneous Self-Assembly of Icosahedral Capsids

Hung D. Nguyen, Vijay S. Reddy, and Charles L. Brooks III*

Department of Molecular Biology, TPC6, 10550 North Torrey Pines Road, La Jolla, California 92037

Received October 18, 2006; Revised Manuscript Received November 21, 2006

ABSTRACT

Self-assembly of viral proteins into icosahedral capsids is an interesting yet poorly understood phenomenon of which elucidation may aid the exploration of beneficial applications of capsids in materials science and medicine. Using molecular dynamics simulations of coarse-grained models for capsid proteins, we show that the competition between the formation of full capsids and nonidealized structures is strongly dependent upon the protein concentration and temperature, occurring kinetically as a cascade of elementary reactions in which free monomers are added to the growing oligomers on a downhill free-energy landscape. However, the insertion of the final subunits is the rate-limiting, energetically unfavorable step in viral capsid assembly. A phase diagram has been constructed to show the regions where capsids or nonidealized structures are stable at each concentration and temperature. We anticipate that our findings will provide guidance in identifying suitable conditions required for in vitro viral capsid assembly experiments.

Introduction. For about half of the known virus families, the protein coat that protects the viral genome, in the form of DNA or RNA, is a "spherical" or icosahedral capsid.[1,2] These capsids are composed of multiples of 60 copies of individual proteins that must assemble correctly, rapidly, and spontaneously on a biological time scale in order to propagate an infection in vivo.[3] Elucidating the means by which viral capsid self-assembly occurs may have potential in assisting the development of novel approaches to interfere with the assembly process and ultimately viral infections. In addition, gaining insights into the capsid self-assembly process may also aid our exploitation of beneficial applications of viral capsids in medicine and materials science. In medicine, empty capsids without the viral genome can be used as a vaccine to prevent cancers; for example, exposure to empty capsids of the human papilloma virus produces antibodies in the body priming an effective immune response in case of subsequent exposure to the infectious virus that causes cervical cancer.[4,5] Also, capsids may be used as carriers in drug delivery because of their ability to specifically target tumor cells; for example, canine parvovirus capsids gain entry into human cells by binding transferrin receptors, which are produced by a variety of tumor cells.[6] In materials science, because of their highly symmetrical monodisperse architectures, viral capsids are versatile nanoscale materials that can be used as templates in catalysis and nanostructure synthesis.[7]

* Corresponding author. Phone: 858/784-8035. FAX: 858/784-8688. E-mail: brooks@scripps.edu.

10.1021/nl062449h CCC: $37.00
Published on Web 01/09/2007

While progress toward understanding the molecular-level mechanisms driving capsid formation has been made through theoretical studies,[8−15] structural analysis,[16,17] and in vitro experiments on the self-assembly of empty capsids using only purified capsids proteins,[11,18,19] relevant atomic-resolution computer simulation studies have been impossible due to the large system sizes required and the long timescales involved although initial attempts are emerging.[20] As a consequence, to-date most simulation studies of capsid formation have been limited to simplified models[21,22] that obscure the geometric nature of the capsid subunits. Because of the importance geometrical factors appear to play, quasi-symmetry and the structural organization of viral capsids is well described by the organization of geometrical shapes into a closed icosahedral structure,[2] these models have not made strong connections to existing experiments on capsid assembly. One inspiring study that did strive to capture the geometrical nature of this problem is by Rapaport et al.,[23,24] who performed the first exploratory molecular dynamics simulations on capsid self-assembly of a polyhedral structure from trapezoidal units. However, they enforced many nonphysical assembly rules ensuring that only full capsids would be formed; therefore, their simulations fail to capture the spontaneous self-assembly process and its dependency on the environment. In this study, we have extended these initial ideas to develop two geometric models that capture geometric and energetic details without any specific built-in self-assembly rules such as a nucleation step; these models

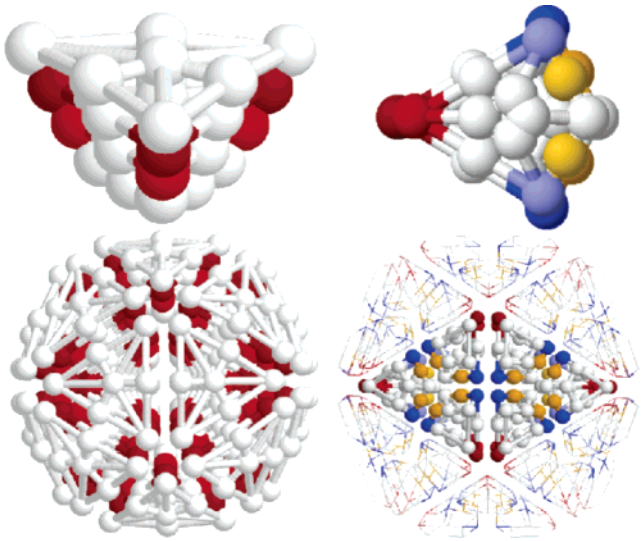

Figure 1. Geometry of our coarse-grained models for (left) a $T = 1$ capsomer and (right) a $T = 1$ structural unit (capsid protein). Covalent bonds are shown between neighboring pseudoatoms. Twenty capsomers or sixty structural units assemble into a complete capsid. Hard pseudoatoms are colored white. For the capsomer model, sites of attraction are colored red. For the structural unit model, interface interactions are between either red or blue pseudoatoms whereas intraface interactions are between yellow pseudoatoms.

are sufficiently simple to allow us to simulate the spontaneous self-assembly of many capsids simultaneously.

The use of geometric models is well suited to study viral capsid self-assembly because of the symmetric nature of spherical viral capsids.[1,2] Our models take advantage of the structural motif that nature has adopted in building protective shells with the largest volume using the minimal number of proteins to cover the surface. In our model, the effective molecular shape is carefully designed to ensure that subunits fit together to form closed icosahedral shells. At the same time, the interactions between subunits are encoded since they are responsible for driving the self-assembly process of viral capsids and maintaining the structural integrity of viral capsids once they are formed. We employ two models with increasing details—one represents a multimer of capsid proteins as a capsomer while the other represents each capsid protein as a single structural unit (Figure 1). Since our results from both models show similar trends, for the sake of clarity we present data only for the capsomer model; data for the structural unit model is included as Supporting Information.

Methods. We consider capsomers comprised of triangular structures designed to assemble into an icosahedron with 20 equilateral triangular faces as shown in Figure 1. In this case, each triangular structure represents a capsomer containing multiple proteins. The capsomers are constructed from four layers of pseudoatoms; each layer is smaller than the next so that when two capsomers are correctly aligned and interacting, their angle is 138.2°. In other words, when assembled, each capsomer's edge is inclined at 20.9° to the normal, resulting in a dihedral angle of 138.2°.

The colored pseudoatoms in the two middle layers signify attractive sites; corresponding pairs of attractive sites on different subunits interact by means of a square-well potential. An interface interaction must involve a square-well potential between a pair of attractive sites that are in the same layer. If two subunits are aligned at the correct angle, they have four square-well interactions (two interactions per corner) and thus their interface is considered "native". Our models also allow the formation of "non-native" contacts; for example, when one subunit is flipped, the two subunits are at a wrong angle with only two square-well interactions and thus their interface is considered "non-native".

We also consider a more detailed model by dividing the above capsomers further into three quadrilateral structural units of the same protein structure as shown in Figure 1. For this model, the assembled polyhedral structure contains 60 quadrilateral structural units occupying 20 triangular faces. There are two types of interactions between attractive sites. Intraface attractions are between yellow pseudoatoms causing the two joining units to form a coplanar aggregate as part of a triangular structure or capsomer as described in the capsomer model above. Interface attractions are between either red or blue pseudoatoms causing the two joining units to form a bent aggregate at a dihedral angle of 138.2°.

Our coarse-grained models capture the essential geometry and interaction details of real capsid subunits yet are simple enough to allow the simulation of systems containing many capsid capsomers, or structural units, and are suitable for use with discontinuous molecular dynamics (DMD),[25−28] an extremely fast alternative to traditional molecular dynamics. In the DMD simulation algorithm, all potentials are discontinuous, i.e., based on hard-sphere or square-well interactions. The solvent is modeled implicitly in the sense that its effect is factored into the energy function as a potential of mean force. The excluded volume of each pseudoatom is modeled using a hard-sphere potential. Covalent bonds are maintained between adjacent pseudoatoms by imposing hard-sphere repulsions whenever the bond lengths attempt to move outside of the range $(1 - \delta)L$ and $(1 + \delta)L$, where L is the bond length and δ represents bond fluctuations and is set to 10% of L. Interactions between attractive sites are represented by a square-well potential of depth ϵ and range 1.5σ, where σ is the pseudoatom diameter. For details of the DMD methodology, see papers by Alder and Wainwright[25] and Smith, Hall, and Freeman.[29]

All simulations were performed in the canonical ensemble with periodic boundary conditions imposed to eliminate artifacts due to the box edges. Constant temperature is achieved by implementing the Andersen thermostat method.[30] Simulation temperature is expressed in terms of the reduced temperature ($T^* = k_BT/\epsilon$, where k_B is Boltzmann's constant, T is the temperature, and ϵ is the basic interaction strength) and reduced time ($t^* = t/\sigma(k_BT/m)^{1/2}$, where t is the simulation time and m is the pseudoatom mass).

The results presented in this paper are averages from many independent simulations using both the capsomer and structural unit models. Since similar results were obtained, here we report our simulation protocols on only the capsomer model. The conditions necessary for capsid formation starting

from isolated and randomly placed capsomers were first explored by performing constant-temperature simulations on a system containing 500 $T = 1$ capsomers, which can potentially form up to 25 complete capsids, over a wide range of temperatures and simulation box sizes; ten simulations were run at each condition. The resulting capsomer concentrations were estimated at $c = 5.41$, 10.82, 21.63, 43.25, 86.5, and 173 μM using the capsomer dimension of ~100 Å, the average length of a trimer occupying a face on crystal structures of small viral capsids.[17] The temperatures were $T^* = 0.25$, 0.275, 0.3, 0.325, 0.35, 0.375, and 0.4 in reduced units. Although each system is relatively large, containing over 14 000 pseudoatoms, our simulations explored the complete assembly process starting from a random configuration and arriving at an equilibrium configuration that exhibits a variety of ordered and disordered structures depending on the simulation conditions. The simulation time required to see the first complete capsid was relatively short, involving only a few days on a single-processor workstation. However, each system was simulated for a long period of time (in total more than ~30 days of CPU time) until the ensemble average of the total potential energy varied by no more than 2.5% during the last three-quarters of each simulation run.

The kinetics of capsid self-assembly was then investigated by conducting 100 constant-temperature simulations at $c = 86.5\mu$M and $T^* = 0.35$, which is the optimal condition for the formation of full capsids, and $T^* = 0.25$, which is the conducive to the formation of mis-assembled structures, on a system containing 500 capsomers. During each simulation, the formation of assembled structures of different aggregate size was monitored as a function of time.

Finally, we performed relatively long equilibrium replica-exchange[31] DMD simulations on six systems containing 500 $T = 1$ capsomers over a very wide range of temperatures and protein concentrations to study the thermodynamics of assembly; simulation of each system took 165 CPU days on an eight-processor cluster. The goal here was to map out a phase diagram in the temperature−concentration plane delineating the regions where different structures of interest are stable and to calculate the free energy associated with each aggregate size in order to elucidate the kinetic mechanism by constructing an energy landscape with the system's free energy as a function of the temperature and average aggregate size using the weighted histogram method.[32]

Results. *Capsid Stability.* Before evaluating the ability of our capsomers model to assemble into polyhedral structures from isolated and randomly placed capsomers, we evaluated the stability of preformed polyhedral structures at various temperatures using the replica exchange method.[31] We examined the effect of variations in the temperature on the populations of the different structural states such as ordered polyhedral structures (complete and partial), disordered aggregates, and free monomers. We observed that the polyhedral structure maintains its integrity at low temperatures, $T^* < 0.40$. At these temperatures, protein subunits in the polyhedral structure fluctuate mildly while conserving their original interactions and inter-subunit distances. At

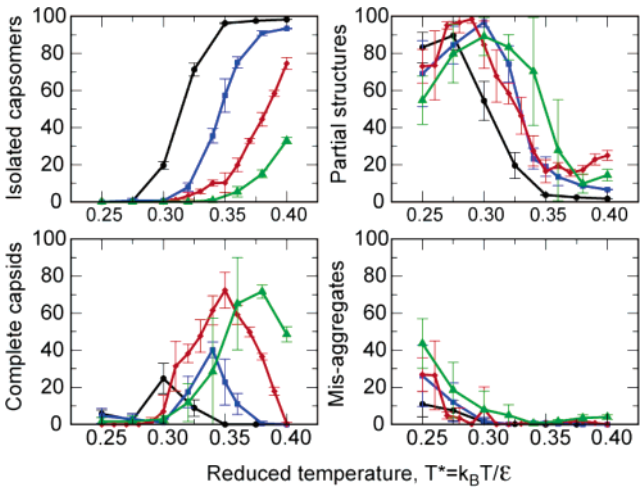

Figure 2. The percentage of capsomers in different structures as a function of temperature, T^*, at different capsomer concentrations: $c = 5.41$ μM (black), 21.63 μM (blue), 86.5 μM (red), and 173 μM (green).

intermediate temperatures $T^* = 0.40-0.45$, the polyhedral structure collapses into an amorphous aggregate, with substantially fewer two-body interactions than in the intact capsid. At high temperatures, $T^* > 0.45$, the capsid disintegrates and its capsomers disperse as indicated by high values of their inter-subunit distance.

Capsid Formation Is a Function of Temperature and Capsomer Concentration. The formation of various structures including complete viral capsid shells depends strongly on the capsomer concentration and temperature[11,19] as illustrated in Figure 2, which shows the percentage of capsomers in various structures as a function of temperature and concentration averaged from our ten simulations at each condition. For each concentration there is an optimal range of temperatures for formation of complete capsids. At the temperatures below this optimal value, instead of complete capsids the system forms either partial capsids or misassembled aggregates (defined below). At temperatures above the optimal range, free capsomers dominate with few forming larger aggregates. At the optimal range of temperature, up to 80% of the total number of capsomers in the system form complete capsids. These optima shift to higher temperatures as the concentration is increased.

Partial structures are isolated and incomplete assemblies containing only native interfaces. Because they are capsid-like and are only one to three capsomers short of becoming complete capsids, they could easily be mischaracterized as complete capsids in experiments.

Since our models allow for the formation of non-native interfaces, we also observe the formation of other aggregates that deviate from ideal capsids. These misassembled structures contain substantially more capsomers than the ideal capsid. They are either closed structures with many non-native interactions (Figure 3a) or open structures that contain a few partial structures (Figure 3b-d). Surprisingly, the geometric organization of these species shows a remarkable resemblance to the "monster particles" observed in experiments by Harrison and co-workers on Turnip crinkle virus.[33]

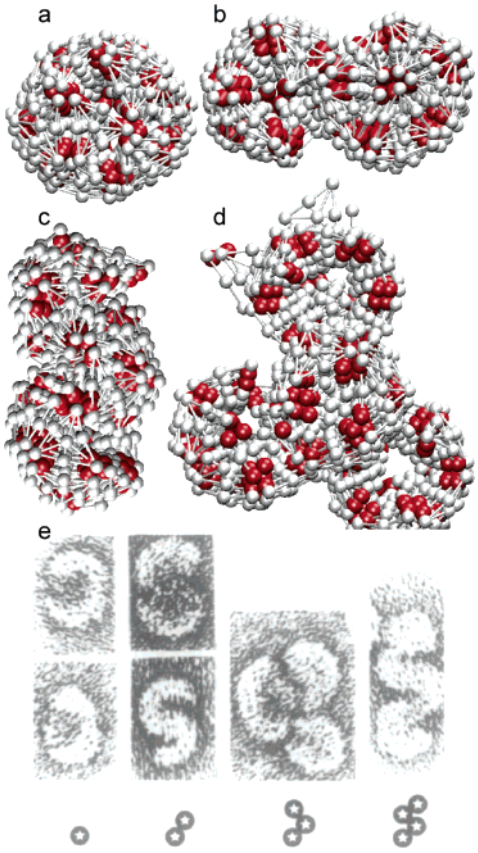

Figure 3. A gallery (top) of oversized misassembled structures, or monster particles, containing an enclosed large aggregate (a) or two (b), three (c), and four (d) open partial capsids and appearing similar to experimentally observed structures (e) from electron microscopy on Turnip Crinkle Virus.[33] The EM images are from Sorger et al. Reprinted from ref 33 with permission from Elsevier. Copyright 1986 Elsevier Ltd.

These structures tend to form at high protein concentrations and especially low temperatures. On the basis of the average number of interactions per protein within these misassembled aggregates, they are energetically less favorable than complete ideal capsids.

Capsid Growth Occurs through Monomer Addition. The kinetic mechanism of capsid self-assembly was investigated in detail by examining the results from 100 constant-temperature simulations at an initial capsomer concentration of $c = 86.5\ \mu$M and temperature $T^* = 0.35$, which represents optimal conditions for the formation of full capsids and are prohibitive conditions for the formation of misassembled aggregates. The average number of aggregates at each aggregate size as a function of time is plotted in Figure 4. Analysis of this figure suggests that capsid self-assembly of simple viruses undergoes continuous growth by adding one monomer (capsomer) at a time rather than by the formation of distinctive intermediates via the collapse of preformed oligomers. In this case, aggregates of low orders exist in small amounts over a very short period of time early in a simulation. In fact, at any time there are about 22 oligomeric intermediates of varying sizes excluding the dimers in the system; interestingly, the number of oligomeric intermediates is less than 25, which is the maximally allowed number of

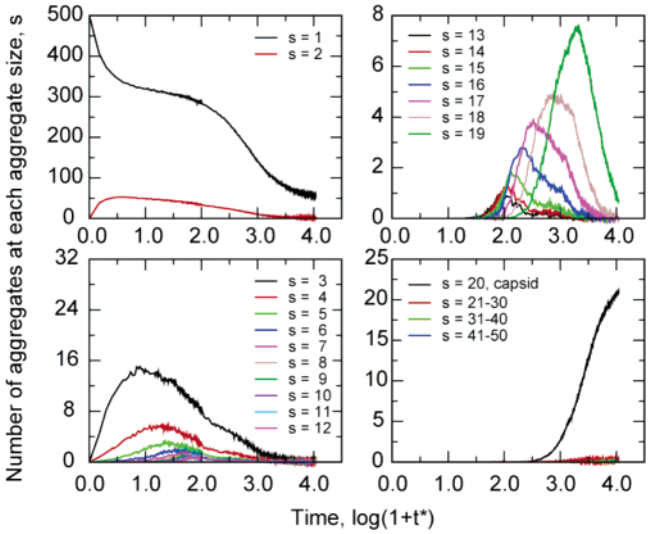

Figure 4. The average number of aggregates at each aggregate size as a function of time, computed from 100 independent kinetic simulations at $c = 86.5\ \mu$M and $T^* = 0.35$.

complete capsids that can be formed given the number of free monomers initially available in this system. Once they are formed, the intermediates are very transient as they proceed to form aggregates of larger sizes and eventually complete capsids. This suggests that the system forms nuclei, each of which is successfully grown gradually into complete capsids, until the concentration of free monomers drops to a certain critical value.

At the end of each simulation, there is a partitioning between complete capsids and free monomers and thus an absence of intermediate sized aggregates. This finding is similarly observed in light scattering and size exclusion chromatography experiments on viral capsid assembly in ref 11. These observations demonstrate that self-assembly of virus capsids is nucleation dependent, which is similar with various experimental studies.[11,19] Our simulations show the characteristic sigmoidal kinetics of capsid formation,[11,12,34,35] which is initiated after a lag time during which intermediates are formed, and followed by a rapid growth phase during which the intermediates become partial and eventually full capsids, and completed in a slow growth phase during which free monomers are depleted.

Our simulation results on the kinetics of capsid formation are in general agreement with those obtained from in vitro experiments[11,18,19] and the two generic thermodynamic-kinetic models (one considered 12 5-fold pentagonal subunits while the other comprised 30 2-fold rectangular subunits) that were developed by Zlotnick and co-workers.[10−12] In these models, icosahedral capsids are formed by successive bimolecular reactions, each of which involves a free monomer and a growing oligomer whose conformation is the maximally stable intermediate based on its energy.[16] Their models assumed that all subunit−subunit interactions and all microscopic forward rates are equivalent. Nucleation was taken into account by imposing rate differences between the nucleation and elongation phases of the reaction. When directly applied to several in vitro assembly systems, these models are successful in identifying key growth features that

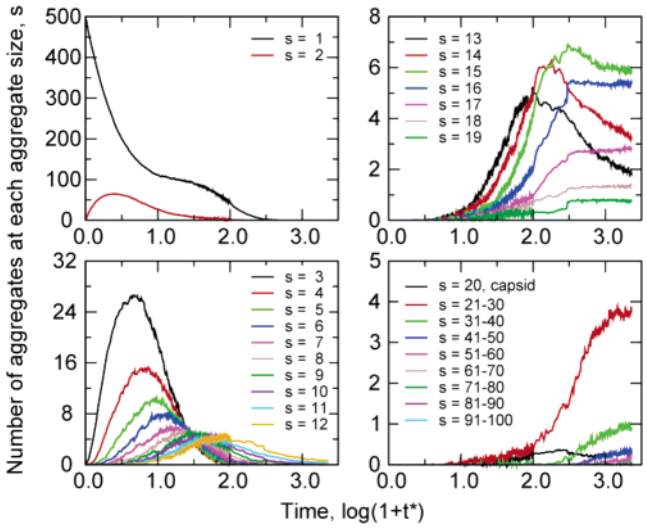

Figure 5. The average number of aggregates at each aggregate size as a function of time, computed from 100 independent kinetic simulations at $c = 86.5\ \mu$M and $T^* = 0.25$.

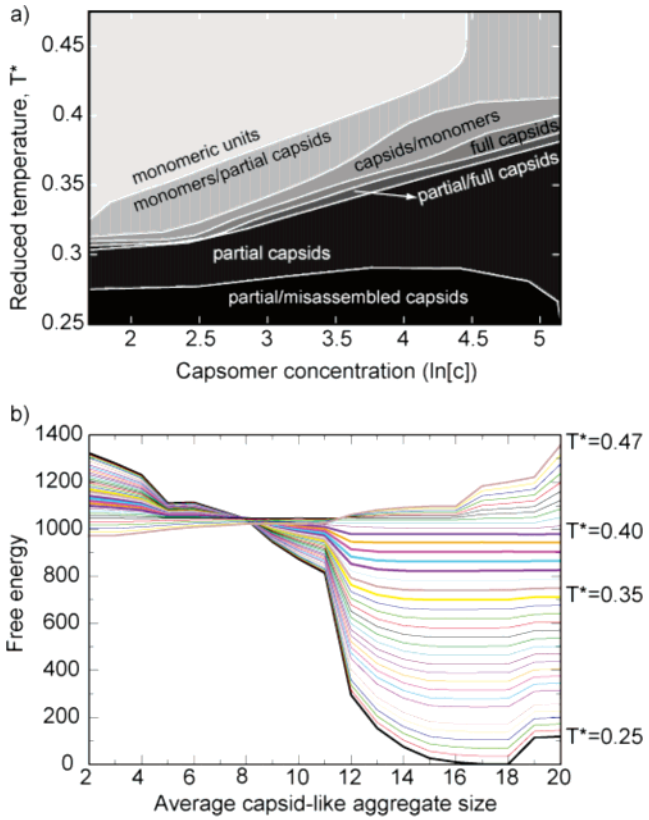

Figure 6. (a) Phase diagram for the 500-capsomer system as a function of the reduced temperature, T^*, and capsomer concentration, c. The single-structure phases are capsids, partial capsids, and free monomers. The two-phase regions are monomers/partial, capsids/monomers, partial/capsids, and monomers/capsids. (b) Free energy associated with each aggregate size as a function of temperature obtained from equilibrium replica-exchange simulations at $c = 173\ \mu$M.

are dependent upon the environmental conditions in the assembly of icosahedral viruses including hepatitis B virus,[11] cowpea chlorotic mottle virus,[18] and polyoma virus.[19]

Monster Particle Growth via Collapse of Preformed Intermediates. Unlike the self-assembly of capsids in which capsid growth occurs through monomer addition, the formation of monster particles that contain a few open partial structures (Figure 3b−d) occurs through the collapse of preformed oligomers of intermediate sizes. This can be seen in Figure 5, which shows the average number of aggregates at each aggregate size as a function of time from 100 constant-temperature simulations at an initial capsomer concentration of $c = 86.5\ \mu$M and temperature of $T^* = 0.25$ (optimal conditions for the formation of misassembled aggregates and prohibitive conditions for the formation of full capsids). Early in simulations, free monomers are rapidly depleted as large populations of oligomers accrue. In fact, at any time there are more than 25 oligomeric intermediates, which independently consume free subunits to grow into large aggregates. Without a sufficient concentration of free subunits, these aggregates either remain as isolated partial capsids throughout a simulation or collapse into oversized misassembled structures. Indeed, nonaveraged time-evolution data on the aggregate size as a function of the temperature for each simulation (not shown) show sharp jumps as oversized misassembled structures are created. This suggests that the system at low temperatures is susceptible to kinetic traps in the sense that assembly is initiated too many times yielding more than enough adequately sized nuclei.[11,36] Once free subunits are depleted, the reactions do not proceed to completion to form capsids; instead, they either remain as partial capsids or join together to form non-native interfaces and create oversized misassembled aggregates.

Monster particles that are enclosed and oversized structures (Figure 3a) often result from the formation of at least one non-native interface during self-assembly. In other words, as a partial structure is grown, a single misstep to form a non-native interface can result in the formation of the wrong curvature. Subsequent addition of monomers closes the structure that contains more than the number of subunits in a complete capsid. We believe that these structures are able to close because the small ($T = 1$) capsids that are being considered here contain subunits that are more likely to form 5-fold symmetry with inward curvature as apposed to more complex capsid architectures ($T > 1$) such as bacteriophage P22 monster particles,[37,38] which contain subunits that are more likely to form 6-fold symmetry with flat curvature.

A Phase Diagram Describing Capsid Self-Assembly. Equilibrium replica-exchange molecular dynamics simulations on systems containing 500 $T = 1$ capsomers over a very wide range of temperatures and protein concentrations were performed to study the thermodynamics of assembly. The goal was to map out a phase diagram in the temperature−concentration plane delineating the regions where free monomers, partial capsids, full capsids, and misassembled aggregates are stable. On the basis of data for the percentage of capsomers that form the various structures, a phase diagram in the temperature−concentration plane was constructed and is displayed in Figure 6a. We found three distinctive single-phase regions: free monomers, partial capsids, and complete capsids. We also found four two-phase regions: monomers/partial capsids, complete capsids/monomers, partial capsids/complete capsids, and partial

capsids/misassembled structures (at each two-phase region, the first species is more prominent than the latter species). The capsid formation region is relatively narrow over the temperature space indicating the delicate stability of empty viral capsids lacking their genomic content. However, partial capsids, which are often experimentally indistinguishable from complete capsids, are stable over a wide region of both the temperature and capsomer concentration spaces.

Misassembled structures are present at equilibrium but in small populations at low temperatures. Compared with the results obtained from our constant-temperature kinetic simulations as seen in Figure 2, the percentage of capsomers that form misassembled structures is smaller. Time−evolution data on the misassembled aggregate size as a function of the temperature (not shown) indicates that many misassembled structures that are formed at low temperatures early in the replica-exchange simulations are unstable and dissolve at higher temperatures.

The Final Addition Step of Capsid Formation Is Rate Limiting. We also constructed an energy landscape with the system's free energy as a function of the temperature and average aggregate size of capsid-like structures as shown in Figure 6b. We observe that at capsid-formation temperatures, self-assembly is a downhill process starting from free monomers situated at the highest free energy at all temperatures and arriving at the global minimum where ordered aggregates of high orders exist. At low temperatures, the free energy of the nearly completed partial capsids is lower than that of the full capsids suggesting that adding one or two capsomers onto partial capsids in order to proceed to completion is disfavored. At intermediate temperatures, the free energy of nearly completed partial capsids is the same as that of the full capsids, meaning that the final addition step is allowed but not favored. Although the final addition step substantially decreases the enthalpy of the system as all interactions by attractive sites in the final subunit are satisfied, the entropic cost is too high as subunits in a nearly completed partial capsid are more flexible than those in a full capsid. In addition, the entropic cost also comes from the fact that the final subunit has to position itself at the right orientation in front of the empty slot before pushing in to form a full capsid.

This finding on the thermodynamics of self-assembly agrees with our kinetic data on the average lifetime of aggregates at each aggregate size (data not shown). We found that the average lifetime of aggregates that contain less than 16 subunits for the capsomer model is statistically equivalent. As aggregates grow into a 17-mer and larger, the average lifetime increases significantly and the amount of time needed for the insertion of the last subunit is the largest compared to other growing steps. This demonstrates that forming partial capsids is a rapid process compared to the final addition steps of incorporating the last subunits into a nearly completed capsid. Therefore, we conclude that the final addition step before completion is rate-limiting. In vivo, the final addition step may be more favorable because of the presence of scaffolding proteins and/or the genome content; our simulations do not provide any insights into the role of putative "assembly assistants".

Conclusions. By combining the discontinuous molecular dynamics technique with our coarse-grained geometric models, we have been able to simulate the spontaneous formation of multiple capsids simultaneously in large systems of many capsomers or structural units starting from random configurations. This enabled us to analyze molecular-level events in the capsid self-assembly process that are difficult or impossible to observe experimentally. The strong competition between the formation non-native structures, such as partial capsids and the monster particles, and the self-assembly of complete capsids was analyzed quantitatively as a function of temperature and concentration. The kinetic mechanism of capsid formation was detailed as a cascade of elementary reactions in which each subunit is added to a growing oligomer. This suggests that it may be possible to inhibit capsid formation by formulating a therapeutic approach that decreases the population of free monomers early in the self-assembly process and increases promiscuous assembly into dead-end products; thus an inadequate concentration of free monomers limits the final addition step from proceeding to completion.

Interestingly, even though our structural unit model contains more details than the capsomer model, the results from the structural unit model exhibit the same behavior as those from the capsomer model. This implies when the initial supply of capsid proteins is limited, as long as subunits are started as either individual proteins or uniform capsomers of the same aggregate size, capsid self-assembly should proceed via the same kinetic mechanism, in which a single subunit is added to the growing oligomers. The alternative mechanism in which preformed oligomers join together to form a complete capsid requires that there exists a stable population of open oligomers with complementary edges and the resulting structure has to contain all capsid-like contacts with either the same number as that or a smaller number than that of a complete capsid. The first case is stochastically less likely to occur than the latter case, which still requires insertion of free monomers into the missing slots in order to form complete capsids. Since we observe that the rate of oligomer growth is much larger than the rate of oligomers collapse, the alternative mechanism is less likely to occur since oligomers tend to become more closed off as each subunit is added and increasingly blocked against joining with other growing oligomers. Perhaps the monomer addition mechanism is universal for only small capsids whereas big capsids containing hundreds of capsid proteins require much longer time for oligomers to grow giving them more time to collapse into one another.

Capsid self-assembly observed in our simulations occurs at conditions that are biologically relevant in both in vivo and in vitro experiments. Specifically, a typical in vitro experiment starts with 20 μM capsid protein,[11,18] which produces comparable yield of viral particles in an HeLa cell for picornaviruses and reoviruses.[39] In addition, our optimal temperature for capsid formation at $T^* = 0.35$ is equivalent to $\sim$308 K, estimated by using the value of -3.5 kcal/mol

as the average inter-subunit contact energy as extracted from experiments on Hepatitis B virus capsids[40] (−3 to −4 kcal/mol) and cowpea chlorotic mottle virus capsids[36] (about −3 kcal/mol). Thus, our range of temperature between $T^* = 0.25$ and 0.50 is equivalent to 220 and 440 K, respectively.

The models that we have developed in this study can be used to further examine the kinetics of viral capsid self-assembly of specific virus systems in which a coat protein has different interaction potentials at each interface. Our ongoing work is taking differential interface potentials into account in models to explicitly examine the role of differential interface potentials on the self-assembly of virus capsids and to see whether the resulting kinetic mechanisms are altered as a result of changes in interface energetics. Our ongoing work also applies the knowledge gained from the development and simulations of self-assembly with the current models to the development of more complicated models that enable formation of capsids containing more than 60 copies of the same proteins.

Acknowledgment. The authors are grateful to Dr. Craig M. Shepherd for stimulating and helpful discussions. This work was supported by the National Institutes of Health through the Center for Multi-Scale Modeling Tools for Structural Biology (RR12255) and the National Science Foundation through the Center for Theoretical Biological Physics (PHY0216576).

Supporting Information Available: A description of our data for the structural unit model is provided. This material is available free of charge via the Internet at http://pubs.acs.org.

References

(1) Crick, F. H.; Watson, J. D. *Nature* **1956**, *177*, 473−475.
(2) Caspar, D. L. D.; Klug, A. *Cold Spring Harbor Symp. Quant. Biol.* **1962**, *27*, 1−24.
(3) Zlotnick, A.; Stray, S. J. *Trends Biotechnol.* **2003**, *21*, 536−542.
(4) Lowy, D. R.; Schiller, J. T. *Biochim. Biophys. Acta* **1999**, *1423* (1), M1−8.
(5) Koutsky, L. A.; Ault, K. A.; Wheeler, C. M.; Brown, D. R.; Barr, E.; Alvarez, F. B.; Chiacchierini, L. M.; Jansen, K. U. N. *N. Engl. J. Med.* **2002**, *347* (21), 1645−1651.
(6) Singh, P.; Destito, G.; Schneemann, A.; Manchester, M. *J. Nanobiotech.* **2006**, *4*, 2.
(7) Douglas, T.; Young, M. *Science* **2006**, *312* (5775), 873−875.
(8) Wales, D. J. *Chem. Phys. Lett.* **1987**, *141*, 478−484.
(9) Berger, B.; Shor, P. W.; Tucker-Kellogg, L.; King, J. *Proc. Natl. Acad. Sci. U.S.A.* **1994**, *91*, 7732−7736.
(10) Zlotnick, A. *J. Mol. Biol.* **1994**, *241*, 59−67.
(11) Zlotnick, A.; Johnson, J. M.; Wingfield, P. W.; Stahl, S. J.; Endres, D. *Biochemistry* **1999**, *38*, 14644−14652.
(12) Endres, D.; Zlotnick, A. *Biophys. J.* **2002**, *83*, 1217−1230.
(13) Bruinsma, R. F.; Gelbart, W. M.; Reguera, D.; Rudnick, J.; Zandi, R. *Phys. Rev. Lett.* **2003**, *90*, 248101.
(14) Zandi, R.; Reguera, D.; Bruinsma, R. F.; Gelbart, W. M.; Rudnick, J. *Proc. Natl. Acad. Sci. U.S.A.* **2004**, *101*, 15556−15560.
(15) Twarock, R. *J. Theor. Biol.* **2004**, *226* (4), 477−482.
(16) Reddy, V. S.; Giesing, H. A.; Morton, R. T.; Kumar, A.; Post, C. B.; Brooks, C. L., III; Johnson, J. E. *Biophys. J.* **1998**, *74*, 546−558.
(17) Shepherd, C. M.; Borelli, I. A.; Lander, G.; Natarajan, P.; Siddavanahalli, V.; Bajaj, C.; Johnson, J. E.; Brooks, C. L., III; Reddy, V. S. *Nucleic Acids Res.* **2006**, *34*, D386−389.
(18) Zlotnick, A.; Aldrich, R.; Johnson, J. M.; Ceres, P.; Young, M. *Virology* **2000**, *277*, 450−456.
(19) Casini, G. L.; Graham, D.; Heine, D.; Garcea, R. L.; Wu, D. L. *Virology* **2004**, *325*, 320−327.
(20) Freddolino, P. L.; Arkhipov, A. S.; Larson, S. B.; McPherson, A.; Schulten, K. *Structure* **2006**, *14*, 437−449.
(21) Zhang, T.; Schwartz, R. *Biophys. J.* **2006**, *90*, 57−64.
(22) Hagan, M. F.; Chandler, D. *Biophys. J.* **2006**, *91*, 42−54.
(23) Rapaport, D. C.; Johnson, J. E.; Skolnick, J. *Comp. Phys. Commun.* **1999**, *121*, 131.
(24) Rapaport, D. C. *Phys. Rev. E: Stat., Nonlinear, Soft Matter Phys.* **2004**, *70*, 051905.
(25) Alder, B. J.; Wainwright, T. E. *J. Chem. Phys.* **1959**, *31*, 459−466.
(26) Rapaport, D. C. *J. Phys. A* **1978**, *11*, L213.
(27) Rapaport, D. C. *J. Chem. Phys.* **1979**, *71*, 3299.
(28) Bellemans, A.; Orban, J.; Belle, D. V. *Mol. Phys.* **1980**, *39*, 781−782.
(29) Smith, S. W.; Hall, C. K.; Freeman, B. D. *J. Comput. Phys.* **1997**, *134*, 16−30.
(30) Anderson, H. C. *J. Chem. Phys.* **1980**, *72*, 2384−2393.
(31) Sugita, Y.; Okamota, Y. *Chem. Phys. Lett.* **1999**, *314*, 141.
(32) Ferrenberg, A. M.; Swendsen, R. H. *Phys. Rev. Lett.* **1989**, *63*, 1195.
(33) Sorger, P. K.; Stockley, P. G.; Harrison, S. C. *J. Mol. Biol.* **1986**, *191*, 639−658.
(34) Prevelige, P. E.; Thomas, D.; King, J. *Biophys. J.* **1993**, *64*, 824−835.
(35) Endres, D.; Miyahara, M.; Moisant, P.; Zlotnick, A. *Protein Sci.* **2005**, *14*, 1518−1525.
(36) Johnson, J. M.; Tang, J.; Nyame, Y.; Willits, D.; Young, M. J.; Zlotnick, A. *Nano Lett.* **2005**, *4*, 765−770.
(37) Earnshaw, W.; King, J. *J. Mol. Biol.* **1978**, *126* (4), 721−747.
(38) King, J.; Griffin-Shea, R.; Fuller, M. T. *Q. Rev. Biol.* **1980**, *55* (4), 369−393.
(39) Zlotnick, A. *J. Mol. Recog.* **2005**, *18*, 479−490.
(40) Ceres, P.; Zlotnick, A. *Biochemistry* **2002**, *41*, 11525−11531.

NL062449H